Sixth International Symposium on Turbulence and Shear Flow Phenomena
Seoul, Korea, 22-24 June 2009

NUMERICAL STUDY OF TURBULENT FLOW PAST AN INCLINED SQUARE CYLINDER

Dong-Hyeog Yoon, Choon-Bum Choi
Department of Mechanical Engineering,
Inha University
Incheon 402-751, Korea

and

Kyung-Soo Yang
Department of Mechanical Engineering,
Inha University
Incheon 402-751, Korea
ksyang@inha.ac.kr

INTRODUCTION

Vortex shedding from a cylindrical object immersed in cross-stream has been one of the popular subjects in fluid mechanics, because it causes periodic force loading on the object, which could have negative effects on the object, such as vibration and noise-generation. Thus large effort has been made by researchers to control the vortex shedding for engineering purposes. Most of work has been focused on flow past a circular cylinder rather than a rectangular one because of its geometrical simplicity (Williamson, 1996; Perry et al., 1982). The main difference between the two is that separation points on a circular cylinder are dynamically determined by the flow field, while they should be fixed on some of the edges of a rectangular cylinder.

A lot of work has been done on flow past a rectangular cylinder aligned with the main flow (Davis and Moore, 1982; Lyn et al., 1995; Obasaju et al., 1990), while relatively less attention has been paid to flow past an inclined rectangular cylinder in literature (Igarashi, 1984; Chen and Liu, 1999; Norberg, 1993; Oudhensden et al., 2005; Taylor and Vezza, 1999). In particular, numerical studies on turbulent flow past an inclined rectangular cylinder are quite rare.

The angle of incidence (θ) of main flow is one of the key factors determining at which edges the flow separates. Change of separation edges inevitably causes change of flow pattern, resulting in change of flow characteristics such as flow-induced forces and Strouhal number (St) of vortex shedding (Igarashi, 1984). Norberg (1993) carried out experimental investigation on the effects of cylinder aspect ratio on pressure forces and vortex-shedding frequencies. Other experimental studies on turbulent flow past an inclined square cylinder include Dutta et al. (2003). Passive flow control has been also attempted to reduce drag on an inclined square cylinder immersed in a main stream (Igarashi, 1996).

In the present numerical investigation, Large-Eddy Simulation (LES) is carried out for turbulent flow past a squre cylinder with various values of θ. The Reynolds number (Re) under consideration is 2,700 based on the cylinder side length (h) and the uniform inlet velocity (U). Based on comprehensive numerical simulations, dependency of flow characteristics on θ will be elucidated, and related flow physics will be explored.

NUMERICAL METHOD AND FLOW PARAMETERS

The box-filtered incompressible continuity and momentum equations, modified for the immersed boundary method (IBM) to implement the cylinder surface, are as follows (Kim et al., 2001);

$$\frac{\partial \bar{u}_j}{\partial x_j} - q = 0 \qquad (1)$$

$$\frac{\partial \bar{u}_i}{\partial t} + \frac{\partial \bar{u}_i \bar{u}_j}{\partial x_j} = -\frac{\partial P}{\partial x_i} - \frac{\partial \tau_{ij}}{\partial x_j} + \frac{1}{Re}\frac{\partial^2 \bar{u}_i}{\partial x_j \partial x_j} + f_i \quad (i = 1, 2, 3) \qquad (2)$$

where $\bar{u}_i$, P, and τ_{ij} represent resolved velocity component in x_i (or x, y, z) direction, filtered pressure, and subgrid-scale stresses, respectively. The terms, f_i, and q were included for IBM, and denote momentum forcing and mass source/sink, respectively. All the physical variables were nondimensionalized by U and h. The governing equations were discretized using a finite-volume method in a nonuniform staggered Cartesian grid system. Spatial discretization is second-order accurate. A hybrid scheme is used for time advancement; nonlinear terms are explicitly advanced by a third-order Runge-Kutta scheme, and the other terms are implicitly advanced by the Crank-Nicolson method. A fractional step method was employed to decouple the continuity and momentum equations. The Poisson equation resulted from the second stage of the fractional step method was solved by a multigrid method. A dynamic subgrid-scale model (Lilly, 1992) was employed for τ_{ij}. For detailed description of the numerical method used in the current investigation, see Yang and Ferziger (1993). The size of the computational domain was set up as $-15 \le x/h \le 20$, $-20 \le y/h \le 20$, $0 \le z/h \le 6$. (Fig. 1) The spanwise length ($6H$) is large enough to contain the important flow structures. A convective boundary condition (Kim et al., 2004) was employed at the outlet. No-slip condition was imposed on the cylinder surface, while flow was assumed periodic in the spanwise direction. On the top and bottom

faces of the computational domain, a slip boundary condition was used. Grid cells were clustered near the solid surface for better numerical resolution, and the number of grid cells was determined by a grid refinement study as 320 × 288 × 64 in the streamwise (x), vertical (y), and spanwise (z) directions, respectively (Fig. 1). The minimum grid spacing on the solid surface is 0.0078h. The angle of incidence was covered from 0° to 45° with increment of 5°.

RESULTS AND DISCUSSION

After the flow became statistically steady, five hundred three-dimensional realizations with a time interval of $\Delta t \approx 0.3h/U$ were collected for statistical analysis. Since the flow was assumed periodic in the spanwise direction, 32,000 two-dimensional fields were actually used for time averaging.

Mean Flow Fields

In Fig. 2, streamlines of the averaged velocity fields are presented for each θ computed. In the case of θ =0° (Fig. 2(a)), flow always separates at the upstream edges (A and B. See Fig. 1), and in addition to the main recirculation bubble behind the cylinder, recirculation regions form on the top and bottom faces of the cylinder without reattachment. As θ increases, however, the recirculation region on the bottom face shrinks (Fig. 2(b)). When θ=15°, it is seen that the flow separated from B reattaches on the bottom face (B-C). As the cylinder is further inclinded (Fig. 2(d)), the reattachment point on B-C moves towards B, revealing a very small recirculation region near the edge B when θ=30° (Fig. 2(e)). In the time averaged velocity fields, the reattachment on B-C occurs in the range of 15°≤θ≤30°. Igarashi (1984) reported that flow separates at B and reattaches on B-C in the range of 14°≤θ≤35°, being in good agreement with our results. Figure 2 also shows that the main recirculation bubble behind the cylinder gets larger as θ increases; this is related to the increasing projected area (H in Fig. 1) with θ, being consistent with the experimental results of Oudheusden et al.(2005).

Phase-averaged streamlines are presented in Fig. 3 for the case of θ=30°. Center points and saddle points are identified in Fig 3(c) as noted by Perry et al. (1982) in their study on the vortex shedding process behind two-dimensional bluff bodies. Flow passage between large vortices (“alleyway”) is also seen. It should be noted that unlike the flow past a circular cylinder, the alleyway flow separates due to the presence of the rear sharp edges (C and D), yielding small vortices near the edges (a and b in Fig. 3(b)). They grow in time (Fig. 3(c)), and finally merge into a big vortex (c in Fig. 3(d)).

Flow –Induced Forces

Time-averaged pressure coefficient $\overline{C_p}$ on the cylinder surface, where $C_p = (P - P_\infty)/\frac{1}{2}\rho U^2$, is presented in Fig. 4 along with the experimental results of Chen and Liu (1999) for various values of θ, while time-averaged drag (C_D) and lift coefficients (C_L) are plotted in Fig. 5, together with the experimental results of Igarashi (1985). In the definitions of both force coefficients, h was used as the length scale. The current numerical results exhibited in Figs. 4 and 5 are in excellent agreement with the experiments. As θ increases, the stagnation point on A-B moves towards B, and pressure on B-C also increases (Fig. 4). In the case of θ=0°, flow separates at A and B, and pressure is low on B-C and A-D due to the recirculation bubbles formed there. When θ=15°, the flow separated at B reattaches on B-C, causing a local pressure increase near the reattachment point (Fig. 4). Since pressure on B-A-D is overall significantly higher than that on B-C-D, the net lift force is downwards (Fig. 5(b)). As the cylinder is further inclinded, the reattachment point on B-C moves towards B. As a result, time-averaged pressure increases on B-C. When θ=45°, flow no longer separates at B, resulting in high pressure on A-B-C (Fig. 4). Consequently, the cylinder experiences high drag force (Fig. 5(a)).

Figure 6 shows St of vortex shedding vs. θ. Here, St_H is based on H and U. Our results are in excellent agreement with experimental data currently available (Chen and Lui, 1999; Norberg, 1993). The Strouhal number steeply increases up to θ=15°, and then gradually decreases with θ. The gradual decrease of St_H can be explained by reattachement of the flow separated at B on B-C (Knisely, 1990; Obasaju et al., 1990). In Fig. 6, St_h is based on h and U. It is seen that St_h becomes the minimum at θ=5°, steeply reaches the maximum at θ=15°, and then gradually decreases up to θ=45°. Igarashi (1984) reported that St_h decreases in the range of 0°≤θ≤7°, but increases in 7°≤θ≤14° due to asymmetric flow pattern. The current numerical results are in good agreement with those of Igarashi’s experiment.

In Fig. 7, variation of time-averaged moment coefficient ($C_m = M/\frac{1}{2}\rho U^2 h^2$) with θ is presented. Here, the positive direction of C_m is defined as the clockwise one. It is seen that negative moment is exerted on the cylinder for all asymmetric flow fields. This is due to the fact that the stagnation point on A-B moves towards B, and the base point on C-D towards D with increasing θ (Figs 2 and 4). C_m reaches the minimum at θ=20°, revealing good agreement with those of other authors (Norberg, 1993; Taylor and Vezza, 1999).

Reynolds Stress Components and Turbulence Intensity

Figures 8 and 9 show time-averaged contours of streamwise and vertical normal components of Reynolds stress, respectively, with increment of 0.04. In Fig. 8, one can notice that strong streamwise fluctuation is associated with flow separation. The highest level of streamwise fluctuation is noticed when θ=0°. As θ increases from 0° to 45°, the component of streamwise normal Reynolds stress drastically reduces near the cylinder. This can be explained by topological change in the flow field. When θ=0°, two separate recirculation bubbles clash at C and D (Fig. 2(a)), promoting streamwise velocity fluctuations. However, when the cylinder is inclined, some of the recirculation bubbles merge into one, resulting in fewer but larger recirculation bubbles (Figs. 2(b) ~ 2(f)) around the cylinder. Such a

topological change significantly reduces velocity fluctuation around the cylinder as seen in Fig. 8. Figure 9 reveals that the component of vertical normal Reynolds stress is rather weak around the cylinder, but strong in the near-wake region due to the main vortex shedding. Since the main recirculation bubbles behind the cylinder get larger with increasing θ, the location of the maximum value is accordingly shifed downstream.

Figure 10 presents contours of time-averaged turbulence intensity ($\overline{u'_i u'_i}/U^2$) in the near-wake region for each θ. Comparison of Figure 10 with Figs. 8 and 9 also confirms that the streamwise fluctuation is dominant around the cylinder while the vertical fluctuation dominates in the near-wake region.

CONCLUDING REMARKS

LES of turbulent flow past a square cylinder immersed in a cross stream at Re=2,700 was carried out to study the effects of its inclination angle with respect to the main flow direction on the flow characteristics such as mean-flow topology, flow-induced forces, vortex-shedding frequency and Reynolds normal stresses, etc.

If the inclination angle is over 15°, flow separated at the lower upstream edge reattaches on the lower side of the cylinder, causing pressure increase on that side leading to high drag and lift coefficients. The recirculation region on the lower side shrinks with increasing inclination angle, and almost vanishes at θ=30°. Counter-clockwise moment is acting on the cylinder when the cylinder is inclined. The maximum magnitude of the moment is identified at θ=20°. It is also found that the streamwise normal component of Reynolds stress is strong around the cylinder, while the vertical normal component is dominant in the near-wake region. Suppression of recirculation bubble on the lower side of the cylinder is responsible for the “laminar” flow there when θ >15°.

ACKNOWLEDGEMENT

This work was supported by UVRC, Korea.

REFERENCES

Chen, J. M., and Liu, C.-H., 1999, "Vortex shedding and surface pressures on a square cylinder at incidence to a uniform air stream," *Int. J. Heat and Fluid Flow*, Vol. 20, pp. 592-597.

Davis, R.W. and Moore, E.F., 1982, "A numerical study of vortes shedding from rectangles," *J. Fluid Mech.*, Vol. 116, pp.475-506.

Dutta, S., Muralidhar, K. and Panigrahi, P.K., 2003, "Influence of the orientation of a square cylinder on the wake properties," *Experiments in Fluids*, Vol. 34, pp.16-23.

Igarashi, T., 1984, "Characteristics of the flow around a square prism," *Bull. JSME*, Vol. 27, pp.1858-1865.

Igarashi, T., 1985, "Heat transfer from a square prism to an air stream," *Int. J. Heat Mass Transfer*, Vol. 28, pp. 175-181.

Igarashi, T., 1996, "Drag reduction of a square prism by flow control using a small rod," *J. Wind Eng. Ind. Aero.*, Vol.69-71, pp.141-153.

Kim, D.-H., Yang, K.-S., Senda, M., 2004, "Large-Eddy Simulation of turbulent flow past a square cylinder confined in a channel, " *Computers and Fluids*, Vol. 33, pp.81-96.

Kim, J., Kim, D., and Choi, H., 2001, "An immersed-Boundary Finite-Volume Method for Simulations of flow in Complex Geometries," *J. Comp. Phys.*, Vol. 171, pp.132-150.

Knisely, C. W., 1990, "Strouhal numbers of rectangular cylinders at incidence: a review and new data," Journal of Fluids and Structures

Lilly, D. K., 1992, "A proposed modification of the Germano subgrid-scale closure method," *Phys. Fluids A*, Vol. 4, pp. 633-635.

Lyn, D. A., Einav, S., Rodi, W., and Park, J.-H., 1995, "A laser-Doppler velocimetry study of ensemble-averaged characteristics of the turbulent near wake of a square cylinder," *J. Fluid Mech.*, Vol. 304, pp.285-319.

Norberg, C., 1993, "Flow around rectangular cylinders: Pressure forces and wake frequencies, " *J. Wind Eng. Ind. Aero.*, Vol. 49, pp. 187-196.

Obasaju, E. D., Ermshaus, R., and Naudascher, E., 1990, "Vortex-induced streamwise oscillations of a square-section cylinder in a uniform stream," *J. Fluid Mech.*, Vol. 213, pp. 171-189.

Oudheusden, B. W., Scarano, F., Hinsberg, N. P., and Watt, D. W., 2005, "Phase-resolved characterization of vortex shedding in the near wake of a square-section cylinder at incidence," *Experiments in Fluids*, Vol. 39, pp. 86-98.

Perry, A. E., Chong, M. S., and Lim, T. T., 1982, "The vortex shedding process behind two-dimensional bluff bodies," *J. Fluid Mech.*, Vol. 116, pp. 77-90.

Taylor, I. and Vezza, M., 1999, "Prediction of unsteady flow around square and rectangular section cylinders using a discrete vortex method," *J. Wind Eng. Ind. Aero.*, Vol. 82, pp. 247-269.

Williamson, C. H. K., 1996, "Vortex dynamics in the cylinder wake, " *Annu. Rev. Fluid. Mech.*, Vol. 28, pp. 477-539.

Yang, K.-S. and Ferziger, J. H., 1993, "Large Eddy Simulation of a turbulent obstacle flow using a dynamic subgrid-scale model, " *AIAA Journal*, Vol. 31, pp.1406-1413.

Sixth International Symposium on Turbulence and Shear Flow Phenomena
Seoul, Korea, 22-24 June 2009

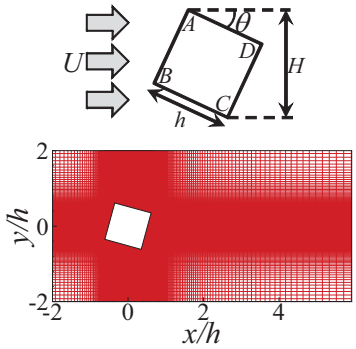

Fig. 1 Flow configuration and grid system.

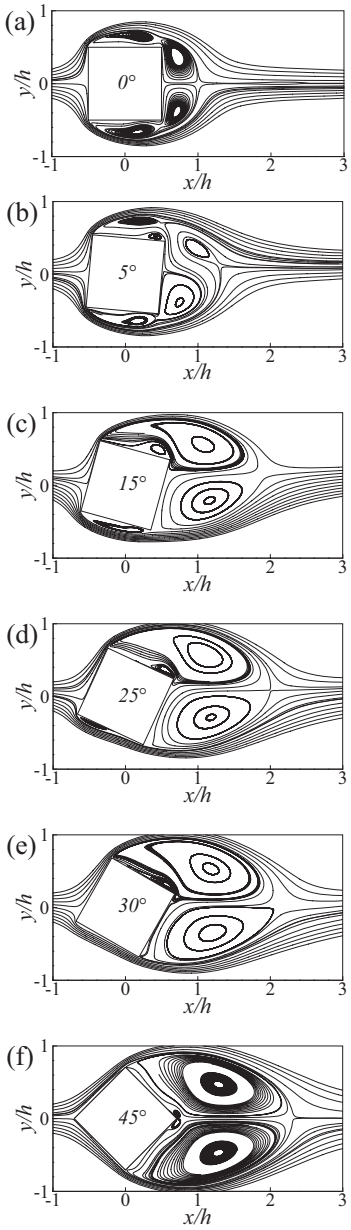

Fig. 2 Streamlines of mean velocity field; (a) θ=0°, (b) θ=5°, (c) θ=15°, (d) θ=25°, (e) θ=30°, (f) θ=45°.

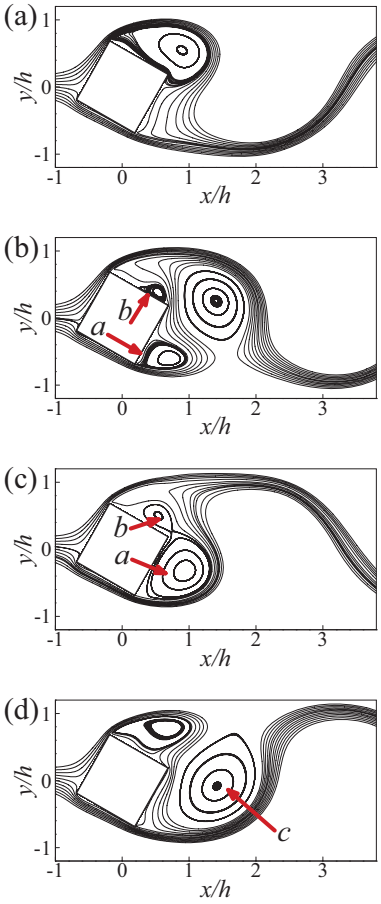

Fig. 3 phase-averaged streamlines for θ=30°; (a) 1/4T, (b) 2/4T, (c) 3/4T, (d) 4/4T, where T is one period of vortex shedding.

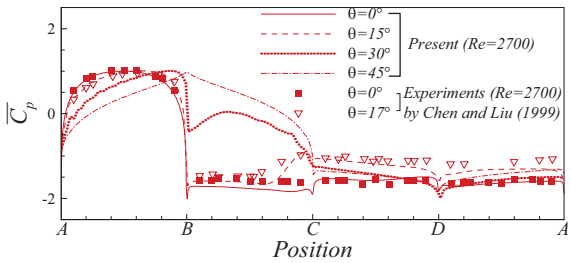

Fig. 4 Distributions of mean pressure coefficient along the cylinder surface, *Re*=2700.

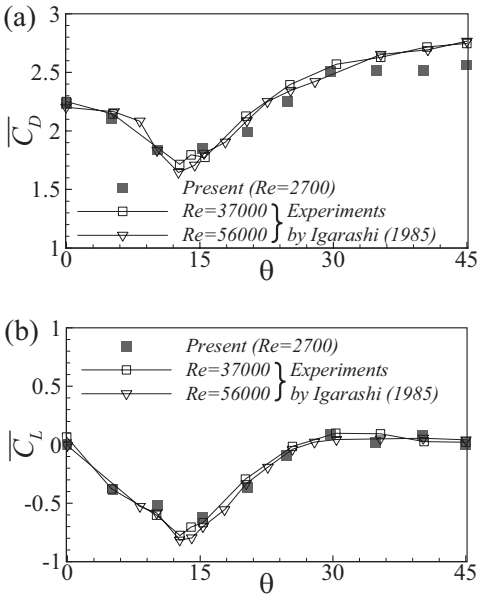

Fig. 5 Time-averaged drag and lift coefficients as the angle of incidence.

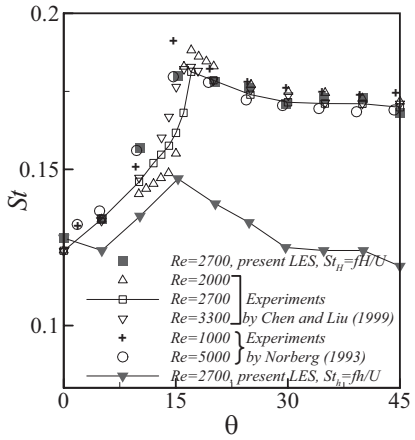

Fig. 6 Strouhal number as the angle of incidence.

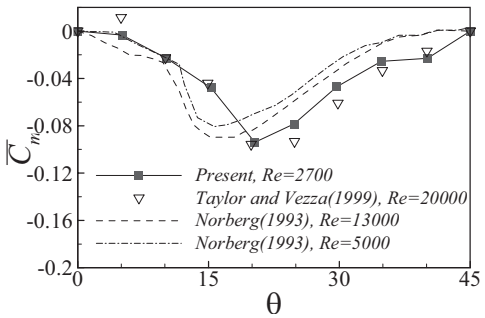

Fig. 7 Variation of moment coefficient with an angle of incidence.

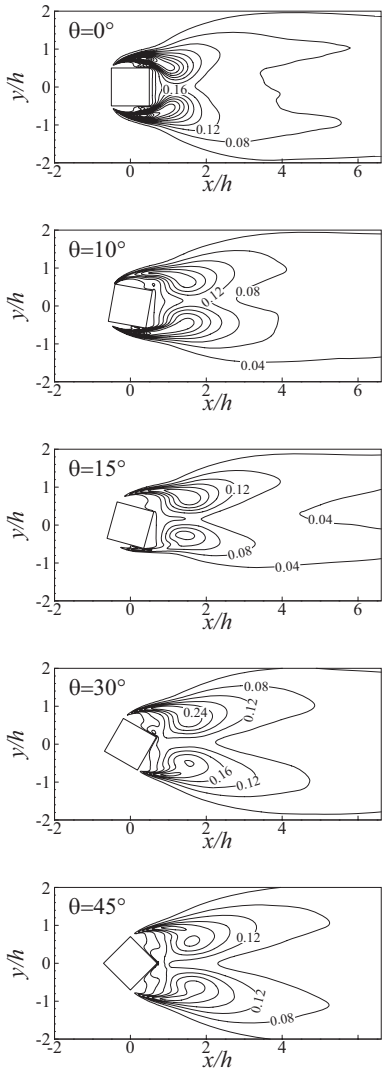

Fig. 8 Contours of streamwise normal stress($\langle u'u' \rangle / U^2$)

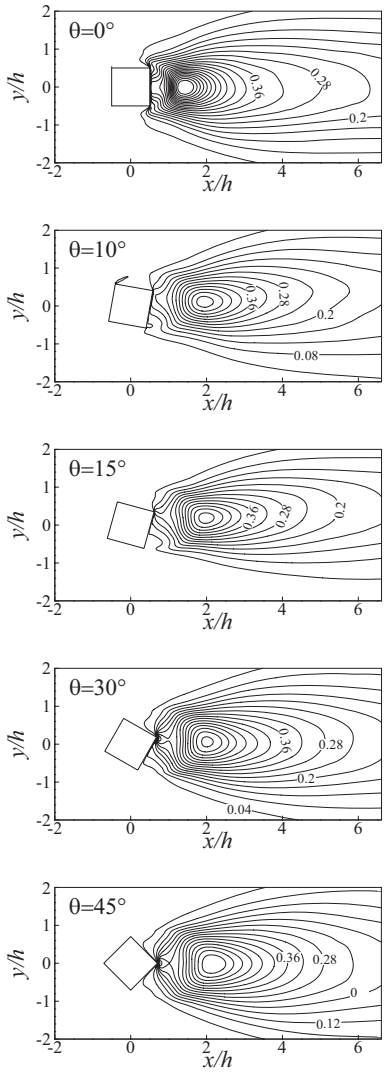

Fig. 9 Contours of streamwise normal stress($\langle v'v' \rangle / U^2$)

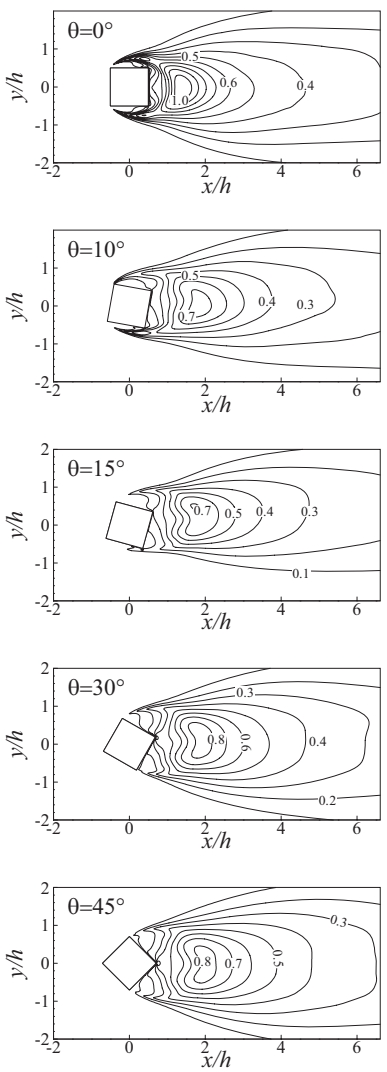

Fig. 10 Contours of turbulent intensity ($\langle u_i'u_i' \rangle / U^2$).